MATERIALS SCIENCE

Solvent-responsive covalent organic framework membranes for precise and tunable molecular sieving

Hao Yang[1,2,3], Haoyuan Zhang[1], Chengjun Kang[1], Chunqing Ji[1], Dongchen Shi[1], Dan Zhao[1]*

Membrane-based nanofiltration has the potential to revolutionize the large-scale treatment of organic solvents in various applications. However, the widely used commercial membranes suffer from low permeability, narrow structural tunability, and limited chemical resistance. Here, we report a strategy for fabricating covalent organic framework (COF) membranes with solvent-responsive structural flexibility. The interlayer shifting of these COF membranes in polar organic solvents results in sub-nanopores with high selectivity. High rejection rates (>99%), high permeance (>15 kilogram meter^{-2} hour^{-1} bar^{-1}), and excellent organic solvent resistance of these smart COF membranes are achieved for a diverse array of nanofiltration applications.

INTRODUCTION

Separation processes are crucial for the modern chemical industry, accounting for over 50% of capital investments (*1*). Organic solvent nanofiltration (OSN) presents a promising and energy-efficient approach to membrane separation, allowing the separation of mixtures to a molecular level and being a potentially disruptive technology in the whole industry chain (*2*, *3*). Nowadays, most OSN membranes are polymeric membranes due to their easy processing and good reproducibility (*4*–*6*). Inorganic membrane materials such as ceramics and zeolites with high chemical stability are also widely used in OSN. However, there are still some challenges in the current polymeric and inorganic membranes for OSN. For instance, additional enhancements are necessary for the permeance and chemical stability of polymeric membranes to meet the practical requirements (*7*–*9*). Inorganic membranes have exhibited exceptional chemical and thermal stability (*10*). However, advanced inorganic membranes with more structural diversity and high mechanical properties need to be further exploited (*11*, *12*).

Smart membranes with stimuli-responsive functions are attractive because they can self-regulate pore sizes under different external conditions (*13*, *14*). Specifically, developing solvent-responsive smart membranes is important since extensive organic solvents are used in OSN. Therefore, it is necessary to develop smart membranes with self-regulated pore sizes, high porosity, and high stability. Covalent organic frameworks (COFs) represent an emerging class of crystalline materials wherein ordered structures are covalently constructed from light element building blocks (*15*–*17*). COFs with highly tailored frameworks and remarkable chemical stability emerge as promising candidates for membrane materials in OSN. In recent years, two-dimensional (2D) COFs have garnered considerable attention due to their precisely arranged pores and exceptional resistance to harsh chemical environments (*14*, *18*–*21*). While covalent bonds link the repeating units within each COF layer, the cohesion between adjacent layers relies on noncovalent forces like π-π stacking and London dispersion. External stimuli have the potential to modulate these physical interactions, consequently leading to changes in the stacking configurations of 2D COFs and bestowing upon them structural flexibility (*18*). Recent investigations have unveiled solvent-triggered interlayer shifting in 2D COFs, transitioning the stacking patterns from AA to quasi-AB stacking when solvated (*22*). The interlayer shifting provides an effective approach for regulating the pore sizes of 2D COFs, demonstrating a high potential for fabricating smart COF membranes for OSN (*13*). However, fabricating highly crystalline 2D COF membranes with interlayer shifting behaviors is challenging because the direct growth of 2D COF membranes usually results in poor crystallinity.

Herein, we report a strategy to fabricate highly crystalline 2D COF membranes with solvent-responsive structural flexibility. These COF membranes demonstrate appropriate sub-nanopores with high selectivity in polar solvents. Ultrafast nanofiltration permeance and high selectivity were obtained by these smart COF membranes during OSN operations.

RESULTS

Preparation of solvent-responsive COF membranes

The COF Tp-TAPT membrane was fabricated by interfacial synthesis using the aldehyde monomer 1,3,5-triformylphloroglucinol (Tp) and the amine monomer 2,4,6-tris(4-aminophenyl)-1,3,5-triazine (TAPT) (Fig. 1A). The Tp and TAPT monomers were mixed in the dichloromethane (DCM) phase underneath the water phase with acetic acid as the catalyst during the synthesis (fig. S1). The COF Tp-TAPT is a typical Schiff-based COF with high chemical stability and outstanding crystallinity, making it a good candidate for preparing smart COF membranes. The synthesized COF Tp-TAPT film shows extremely sharp powder x-ray diffraction (PXRD) peaks (fig. S2). Fourier transform infrared spectroscopy (FTIR) was used to characterize the chemical structures of these COF membranes (fig. S3). The COF Tp-TAPT membrane was obtained through a vacuum-assisted filtration of thin COF film onto a polydopamine-modified polyvinylidene fluoride (PVDF) substrate. The thickness of the COF Tp-TAPT layer is around 150 nm, which was determined by cross-sectional field-emission scanning electron microscopy (FESEM) and atomic force microscopy (AFM), as shown in Fig. 1 (B to D). The surface of the COF Tp-TAPT membrane is smooth and defect free (Fig. 1E), and the roughness parameters R_a and R_q are as low as 0.64 and 0.735, respectively, calculated by the 3D AFM analysis. The ordered crystalline structure of the COF

[1]Department of Chemical and Biomolecular Engineering, National University of Singapore, 4 Engineering Drive 4, Singapore 117585, Singapore. [2]State Key Laboratory of Pollution Control and Resource Reuse, School of the Environment, Nanjing University, Nanjing 210023, China. [3]Institute for the Environment and Health, Nanjing University Suzhou Campus, Suzhou 215163, China.
*Corresponding author. Email: chezhao@nus.edu.sg

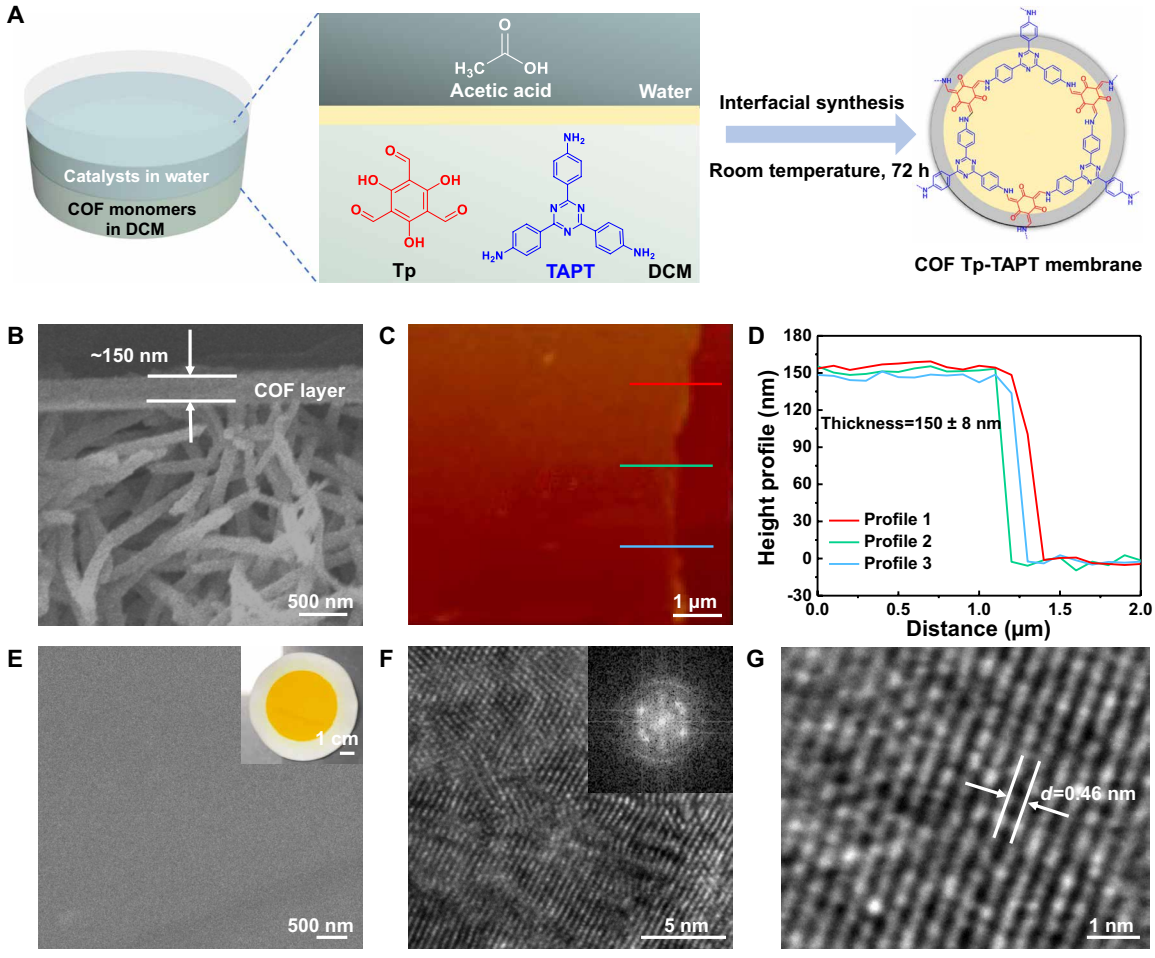

Fig. 1. Preparation and characterization of COF Tp-TAPT membranes. (**A**) Schematic of the fabrication of the COF Tp-TAPT membrane. (**B**) Cross-sectional FESEM image of the COF Tp-TAPT membrane. (**C**) AFM image and (**D**) the height profile of the COF Tp-TAPT film. (**E**) Surface FESEM image of the COF Tp-TAPT membrane inserted with an optical image of the membrane. (**F** and **G**) High-resolution FETEM images of the COF Tp-TAPT film inserted with a fast Fourier transform image. h, hours.

Tp-TAPT film was observed by field-emission transmission electron microscopy (FETEM), in which the lattice fringes with a *d*-spacing of 0.46 nm correspond to the (001) plane (Fig. 1, F and G).

Characterization and simulations of solvent-responsive COF membranes

Molecular simulations were conducted to further investigate the crystallographic structures of the synthesized COF Tp-TAPT film. A comparison of the experimental PXRD patterns of the COF Tp-TAPT film with those of COF powders synthesized via conventional solvothermal methods, characterized by AA stacking structures, reveals disparities in peak quantity, peak position, and relative peak intensity (fig. S4). This structure closely resembles quasi-AB stacking structures (Fig. 2A). Characterization of the solvated COF film samples was conducted to study the interlayer shifting behaviors of the COF membranes. The used solvents cover a wide range of polarity (fig. S5). Obvious disparities in the PXRD patterns were promptly observed when the COF Tp-TAPT films were solvated by polar solvents, including *iso*-propanol, ethanol, dimethylformamide (DMF), chloroform, tetrahydrofuran (THF), DCM, acetone, and methanol. Notable alterations in the relative peak intensity, especially between the (100) peaks and other peaks, were observed. For dried COF Tp-TAPT, the (100) peak at 6.3° displayed an intensity roughly 1.6 times higher than that of the (110) peak at 11.7°. However, upon solvation by polar organic solvents, the intensity of the (100) peak compared to the (110) peak decreased to 0.7-fold. The PXRD results indicate that the COF Tp-TAPT films have solvent-responsive structural flexibility.

To understand the structural changes at a molecular level, molecular simulations were used to identify potential structures that best match the experimental PXRD data (Fig. 2B). The Pawley refinements produce outstanding matches between the experimental and simulated results, thereby robustly confirming the validity of the modeled structures. These structural findings suggest an increased significance of interlayer shifting following solvation by polar solvents. The simulations demonstrate that the adjacent layers of Tp-TAPT shift along the zigzag direction from 4.6 to 7.1 Å when solvated by ethanol (Fig. 2C). COF Tp-TAPT film in polar organic solvents could exhibit an almost AB-stacked structure (circular pore shape) with a smaller pore size of 4.7 Å compared to the AA-stacked structure (circular pore shape, 14.0 Å) or the quasi-AB–stacked structure (oval pore shape, 12.2 Å), suggesting high potential in precise

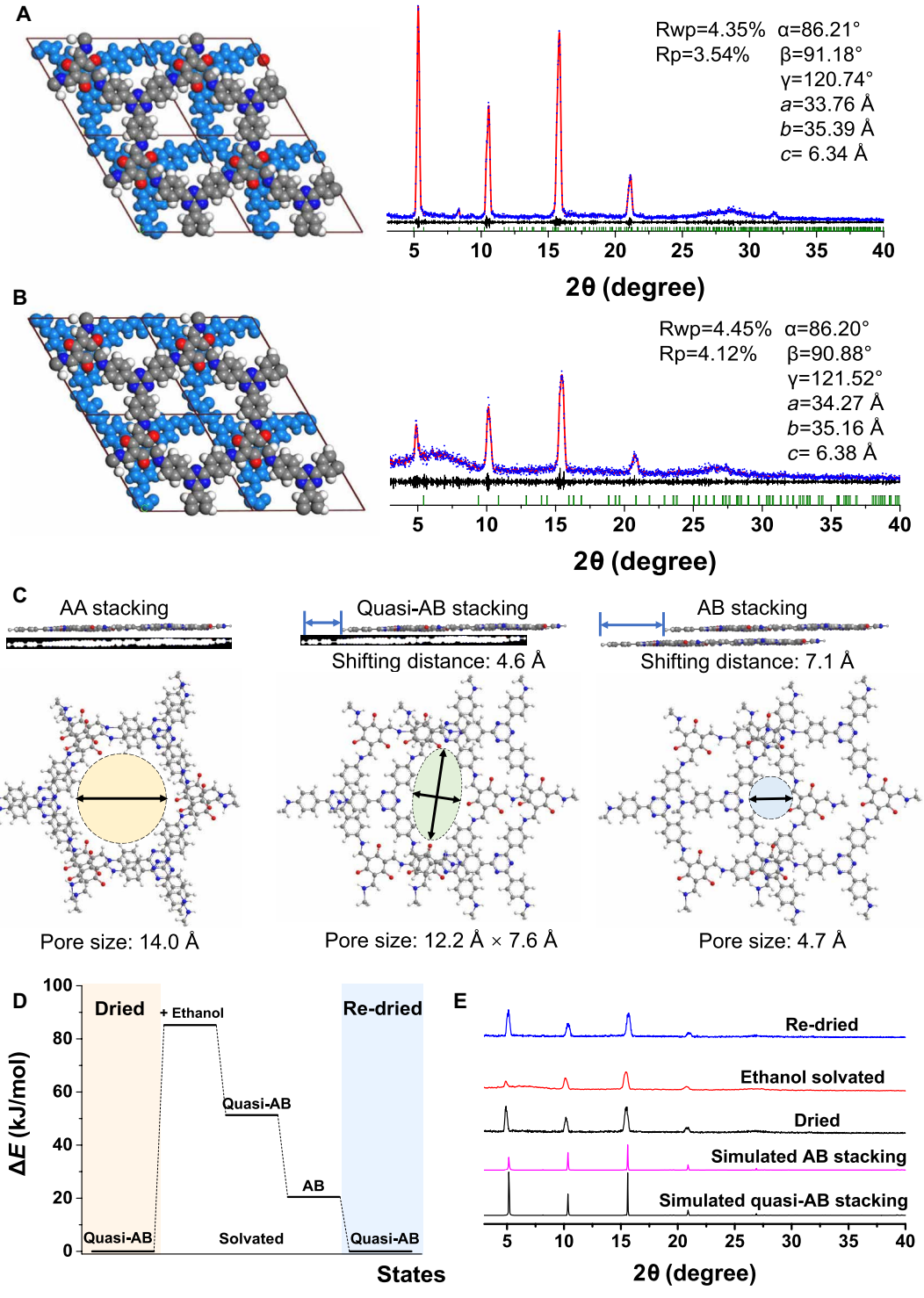

Fig. 2. Simulations of structural changes of solvated COF Tp-TAPT films. Pawley refinement of (**A**) dried (quasi-AB stacking) and (**B**) solvated (AB stacking) COF structures. Red, simulated PXRD patterns; blue, experimental PXRD patterns; gray, difference between simulations and experimental data; green, Bragg conditions. (**C**) Simulated structures showing the interlayer shifting and COF pore size change among AA, quasi-AB, and AB stacking. (**D**) Energy landscape of COF Tp-TAPT computed using DFT. (**E**) PXRD patterns of COF Tp-TAPT film in dried, solvated, and re-dried states.

molecular separation. The PXRD patterns of the COF Tp-TAPT films showed no obvious change when solvated by nonpolar organic solvents [carbon tetrachloride (CTC), cyclohexane, *n*-heptane, and *n*-hexane], low-polarity organic solvents (ethyl acetate and toluene), and water, which could be attributed to the weak interactions between the COF Tp-TAPT and these solvents. We measured the water vapor adsorption-desorption isomers of the COF Tp-TAPT, as shown in fig. S6. The COF Tp-TAPT shows a low water vapor uptake of 0.0851 g g^{-1}, indicating the low affinity between COF Tp-TAPT and water molecules. Although water is a highly polar solvent, it cannot trigger interlayer shifting because of the weak interactions between water and COF Tp-TAPT.

To probe the thermodynamics of interlayer shifting in COF Tp-TAPT film, density functional theory (DFT) calculations were conducted on a COF Tp-TAPT and ethanol system (Fig. 2D). The energy of Tp-TAPT under different states was calculated. The energy of quasi-AB–stacked Tp-TAPT in ethanol (51.3 kJ/mol) is higher than that of AB-stacked Tp-TAPT (20.8 kJ/mol). Therefore, from a thermodynamic standpoint, AB-stacked mode is favored over quasi-AB–stacked mode in ethanol. Subsequently, the reversibility of interlayer shifting was investigated by measuring the dried, solvated, and re-dried COF Tp-TAPT film samples. Our findings demonstrate that the dried COF Tp-TAPT film could fully revert to its previous quasi-AB stacking with high crystallinity (Fig. 2E). Besides ethanol, the interlayer shifting behaviors triggered by other polar organic solvents are also reversible (fig. S7). The large π-conjugated structure of COF Tp-TAPT film with strong interlayer interactions affords regularly stacked structures, promoting high crystallinity and maintaining reversibility during the interlayer shifting processes.

OSN by solvent-responsive COF membranes

The solvent transport behaviors were studied by plotting and fitting the solvent permeance against solvent viscosity or combined solvent property parameters (Hansen solubility parameter, viscosity, and molar diameter) (table S1). The Hansen solubility parameter is a numerical value that indicates the relative solvency behavior of a specific solvent. It is a metric measuring the cohesive energy between molecules. For nonpolar organic solvents, low-polarity organic solvents, and water, the permeance was found to be linearly proportional to the combined solvent property parameter $\delta_0\ \eta^{-1}$, where δ_0 represents the total solubility parameter and η denotes the solvent viscosity (Fig. 3A and fig. S8). The pore size of the COF Tp-TAPT membrane could change from 12.2 Å to 4.7 Å in polar organic solvents, making steric hindrance a plausible factor. On the basis of the pore flow mechanism, Wang *et al.* (*23*) and He *et al.* (*24*) recently proposed a method to bring the sizes of solvent molecules into mechanistic fitting, which related the solvent permeance to membrane pore size, kinetic diameter of solvent molecules, and solvent viscosity. According to this correlation, a good fitting of the solvent permeance to a model parameter $d(d - d_m)^2\eta^{-1}$ was obtained (fig. S9), where d is membrane pore size and d_m is solvent molar diameter. This result indicates that the pressure-driven flows of polar solvents essentially obey the classic pore flow mechanism. Besides, the permeance of polar solvents also exhibited a linear relationship with another parameter $\delta_0\ \eta^{-1}\ d_m^{-2}$ (Fig. 3B and fig. S10). Including d_m term into transport analysis is essential as it signifies the molecular steric effect within enhanced confinement. We demonstrate that solvent permeance is influenced by solvent viscosity and the affinity of the solvent to the membrane. On the basis of the recent physical basis for solvent flow in OSN by Fan *et al.* (*25*), our results strongly support the pore flow transport of solvents in membranes. In addition, the pressure-driven solvent transport in membranes is governed by viscous flow and not by diffusion.

We assessed the dye rejection performance of the COF Tp-TAPT membranes to explore their molecular weight cutoff (MWCO) using aqueous solutions containing three organic dyes—acid fuchsin (585.5 Da), Congo red (696.7 Da), and methyl blue (799.8 Da)—each at a concentration of 50 parts per million (ppm). It should be noted that all the feed solutions with a concentration of 50 ppm are homogeneous solutions. The rejection rates of those three dyes in water were moderate. However, when changing the solvents from water to polar organic solvents, the rejection for all dyes increased substantially (figs. S11 to S14). In particular, the rejection of acid fuchsin could be elevated from 53% to 95% when changing the solvent from *n*-hexane to ethanol. The effect of pressure on membrane separation performance was determined, as shown in fig. S15. The flux is nearly linear to the applied pressure. Both the permeance and acid fuchsin rejection are steady with increasing operating pressure from 2 bar to 6 bar, indicating the highly compact resistance of the membranes.

The rejection rates of methyl blue in different polar solvents are all higher than 99%. The Tp-TAPT membrane was further used for rejecting smaller dyes, including methyl orange (327.3 Da) and acid blue 25 (416.4 Da), in polar organic solvents (figs. S16 and S17). High rejection rates of 96% and 99% were obtained for rejecting methyl orange and acid blue in ethanol, respectively. We further studied the effect of the polarity gradient of the solvents on the membrane performance (Fig. 3C). The mixed solvents of water/ethanol or *n*-hexane/ethanol were used to test the membrane performance. With the increase of ethanol concentration in the solvent, the rejection of acid fuchsin gradually increased while the permeance decreased. This phenomenon further confirms that the COF Tp-TAPT membranes have solvent-responsive structural flexibility, which decreases pore size in polar organic solvents by interlayer shifting. It is worth noting that although the permeance decreases in ethanol (from 33 to 18 kg m^{-2} $hour^{-1}$ bar^{-1}), it is still two magnitudes higher than that of the conventional polymeric membranes (*3*). In addition, the MWCO could be reduced from about 800 Da to 320 Da when changing the nonpolar organic solvents to polar organic solvents (fig. S18), indicating that the pore sizes of these COF membranes could be effectively tailored by solvent-induced interlayer shifting to meet the different requirements in OSN. The responsive tunability of the COF Tp-TAPT membrane performance was studied by alternately testing the dye rejection in ethanol and *n*-hexane over five cycles (Fig. 3D). The results show that the rejection in both ethanol and *n*-hexane are steady over five cycles, indicating the good structural reversibility of the COF Tp-TAPT membranes. Furthermore, the long-term stability of the membrane performance was tested in DMF, and the COF Tp-TAPT membrane performance could be stable for up to 7 weeks (Fig. 3E). The steady permeance in the cyclic test underscores the superior anti-fouling properties of COF Tp-TAPT membranes. The chemical stability of the COF Tp-TAPT membranes was further tested by soaking them in strong acid and alkali solutions for 2 weeks (figs. S19 and S20). There were no obvious changes in PXRD patterns, indicating good chemical stability.

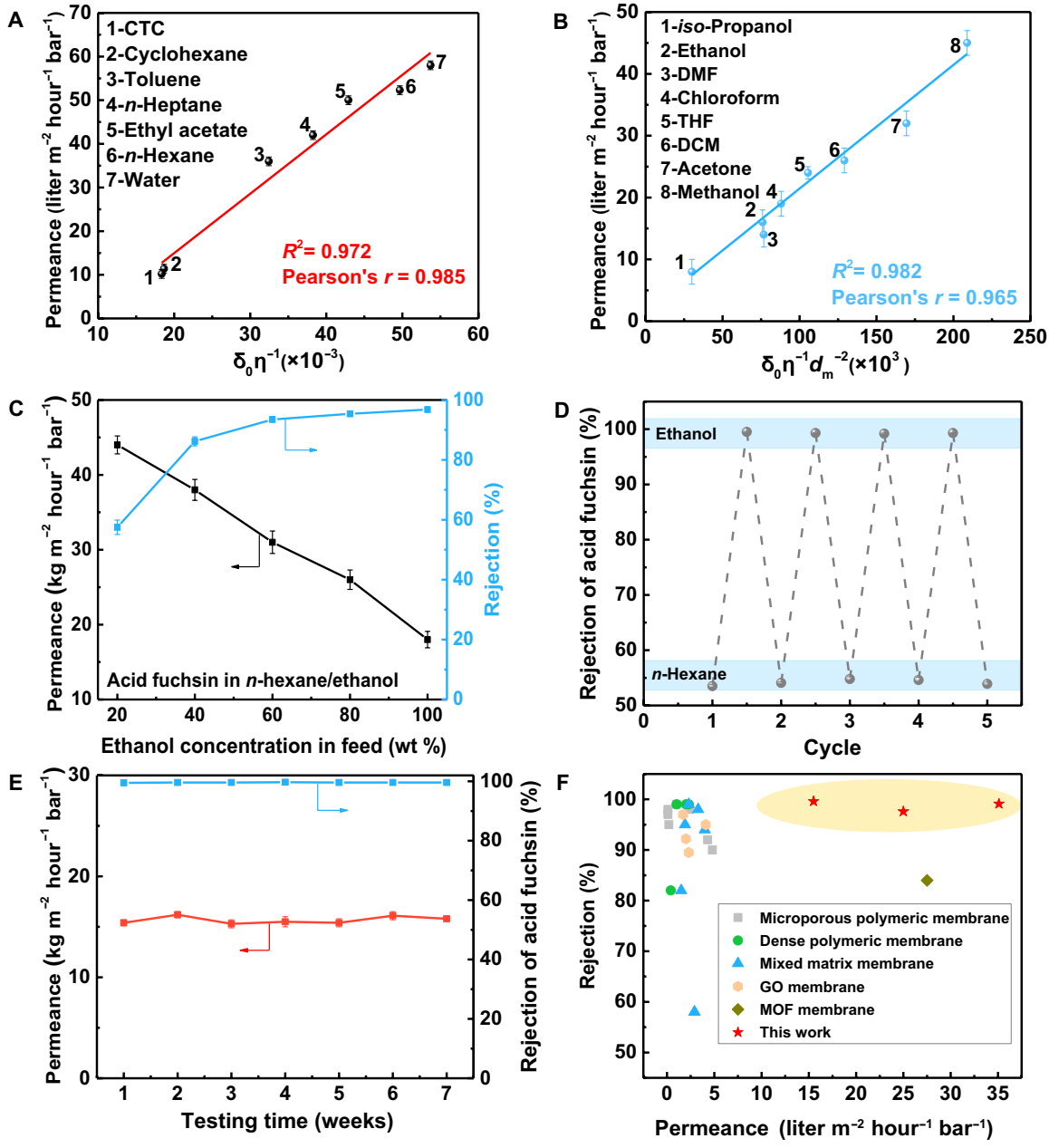

Fig. 3. Separation performance of COF Tp-TAPT membranes. (**A**) Solvent transport through COF Tp-TAPT membrane in nonpolar organic solvents, low-polarity organic solvents, and water. (**B**) Solvent transport through COF Tp-TAPT membrane in polar organic solvents. (**C**) Dye rejection performance of COF Tp-TAPT membrane using the feed with different polarity gradients. (**D**) Responsive tunability of COF Tp-TAPT membrane performance in polar and nonpolar organic solvents. (**E**) Long-term stability of COF Tp-TAPT membrane for rejecting acid fuchsin in DMF. (**F**) OSN performance comparison of the solvent-responsive COF membranes in this work to the state-of-the-art membranes in the literature for rejecting solutes with molecular weights of 580 to 800 Da.

Besides dye rejection, the COF Tp-TAPT membranes were also used to separate high-value-added products such as active pharmaceutical ingredients (APIs) and homogeneous catalysts. Three kinds of value-added APIs, curcumin (368 Da), tetracycline (444 Da), and chlorophyll (893 Da), were selected for the OSN performance test of these COF membranes. The rejection of curcumin experienced a notable increase from 37% to 92% when transitioning from nonpolar solvents to polar organic solvents, mirroring the trend observed in dye rejection (fig. S21). A steady permeance higher than 20 kg m^{-2} $hour^{-1}$ bar^{-1} was obtained for a long-term chlorophyll rejection test (figs. S22 and S23). The COF membranes were further used to recover homogeneous catalysts, as most noble metal–based homogeneous catalysts widely used in industry are expensive. High rejection rates of >90% were achieved for rejecting Hoveyda-Grubbs Catalyst M720 (626.6 Da), tris(2,2′-bipyridine)ruthenium(II) hexafluorophosphate (859.6 Da), and $(Ir[dF(CF_3)ppy]_2(dtbpy))PF_6$ (1121.9 Da) in polar organic solvents (figs. S24 to S27). In practical chemical syntheses, the mixed organic solvents are usually used. For example, in the synthesis of

API [6-chloro-2-(4-chlorobenzoyl)-1*H*-indol-3-yl]-acetic acid, the mixed solvents of ethanol and DMF were used (*26*). As a case study, we investigated the recovery of homogeneous catalysts $Pd(OAc)_2PPh_3$ by the COF membranes in mixed DMF/ethanol solvents, with the DMF concentration varying from 20 to 100 wt %. The membrane permeance gradually decreased (from 24 to 12 kg m^{-2} $hour^{-1}$ bar^{-1}), while the rejection gradually increased (from 85 to 98%) with the increase of DMF concentration in the feed (fig. S28). The results highlight the promising potential of these COF membranes for practical separation applications, particularly in scenarios involving solvent polarity changes.

In addition to OSN, the organic solvent reverse osmosis (OSRO) performance of the COF Tp-TAPT membranes was also evaluated to study the impact of membrane pore size change. Since biofuel upgrading is an important industrial separation process for biofuel production, the continuous separation performance tests of three kinds of 50/50 wt % alcohol/water, including ethanol/water, *iso*-propanol/water, and *n*-butanol/water, were performed (fig. S29). During the separation process, water gradually permeated through the membranes, leading to the solvent polarity change of the alcohol/water mixture. The solvent polarity change triggered the interlayer shifting of COF Tp-TAPT membranes, reducing the membrane pore size. Therefore, the water selectivity was enhanced within the separation time. Using ethanol/water mixture as an example, the obvious peak intensity decrease of the (100) plane was observed when increasing the ethanol concentration in the mixed solvents, indicating that the pore structures of COF Tp-TAPT are different in the solvents with different polarity gradients (fig. S30). The molecular dynamics (MD) simulations based on the experimental results were conducted to demonstrate the dynamic change of the COF Tp-TAPT structures during the separation process. For the ethanol concentrations of 25, 50, 75, and 100 wt % in the mixed solvents, the interlayer shifting distance of COF Tp-TAPT is 5.3, 6.0, 6.6, and 7.1 Å, respectively (fig. S31). Therefore, the pore size of COF Tp-TAPT membranes gradually decreased from ~9.5 Å to 4.7 Å during the separation process, resulting in high water/alcohol selectivity. The water concentration in permeate was higher than 94 wt % after continuous separation of 10 hours. The DMF and ethyl acetate dehydration performance was also tested by the COF Tp-TAPT membranes since the purification of these organic solvents is widely demanded in the industry (figs. S32 and S33). In a continuous separation of 50/50 wt % DMF/water, a separation factor of higher than 15 was obtained. The findings underscore the substantial potential of these solvent-responsive COF membranes for industrial liquid mixture separation via OSRO at low operating pressures.

To investigate the universality of the methods for preparing solvent-responsive COF membranes, we further synthesized two other COF membranes, i.e., COF Tp-TAPA [tris(4-aminophenyl)amine] and COF Tp-DAP (1,6-diaminopyrene) membranes (figs. S34 and S35). Similar to the COF Tp-TAPT membrane, these two COF membranes also exhibited high crystallinity and interlayer shifting behaviors in polar organic solvents (figs. S36 to S39). The notable MWCO change of these two COF membranes was also observed by dye rejection tests in different solvents (figs. S40 and S41). These results demonstrate that the approach used in this study to prepare smart COF membranes is universal. A 7-week test of COF Tp-TAPA and COF Tp-DAP membranes for rejecting dyes in DMF illustrates their remarkable stability for separation tasks involving aggressive organic solvents (figs. S42 and S43). Furthermore, the performance of these solvent-responsive COF membranes surpasses that of state-of-the-art polymeric membranes, mixed matrix membranes, graphene oxide (GO) membranes, metal-organic framework (MOF) membranes, and commercial nanofiltration membranes (*8*, *27*–*55*), underscoring their potential for precise and tunable molecule sieving (Fig. 3F).

DISCUSSION

In summary, this study represents smart 2D COF membranes with solvent-responsive structural flexibility. We successfully fabricated a range of solvent-responsive COF membranes using a universal interfacial synthesis approach. The structural changes of 2D COF membranes in solvents were investigated. These solvent-responsive COF membranes demonstrated high permeance, good rejection, and long-term stability for OSN applications. Notably, the membranes exhibited two orders of magnitude higher permeance compared to traditional polymeric membranes, making them well suited for industrial OSN processes. Our results indicate that solvent-responsive structural flexibility has an immense impact on membrane permeability and selectivity, which may inspire future research on designing high-performance porous membranes based on framework dynamics.

MATERIALS AND METHODS

Characterization methods

SEM images of the membranes were observed via a field-emission scanning electron microscope (JSM-7610F, JEOL). The crystal phase was characterized by XRD on an x-ray powder diffractometer (Rigaku MiniFlex 600) with a Cu sealed tube ($\lambda = 1.540598$ Å) at a scan rate of 3° min^{-1}. FTIR spectra were obtained with a Nicolet 6700 FTIR spectrometer. The ultraviolet-visible (UV-Vis) absorption spectra were tested through an Agilent Cary 60 instrument. Microstructural characterizations of COF films were conducted by atomic force microscope (Bruker) under a tapping mode and high-angle annular dark-field (JEM-ARM200F, JEOL) microscope equipped with an ASCOR aberration corrector and a cold-field emission gun at 200 kV. TEM images were collected on a JEOL JEM-2100F instrument.

Preparation of polydopamine-modified PVDF substrates

The PVDF substrates were modified by using dopamine according to the reported literature (*56*). In detail, a dopamine/tris-HCl (pH 8.5) solution (2 mg ml^{-1}) was prepared. The solution was then poured onto the PVDF surface at room temperature. The dopamine-modified PVDF substrates were obtained after 20 hours of dopamine solution treatment and stored within deionized water before use.

Preparation of COF membranes

A 50-ml mixture comprising TAPT (10 mM), Tp (10 mM), and DCM was poured into a beaker. Then, water (100 ml) was dropwise added onto the surface of the DCM phase. After that, acetic acid (1 ml, 0.6 mM) was dropped in the water phase. The system was kept static for 72 hours to synthesize the COF Tp-TAPT film at the water-DCM interface. The COF Tp-TAPT film was transferred onto a polydopamine-modified PVDF substrate by vacuum filtration to obtain the COF Tp-TAPT membrane. The as-prepared membranes were dried in a vacuum oven at room temperature for 3 hours and

then immersed into THF for 12 hours. The membranes were removed from THF and then washed with ethanol to obtain the final COF Tp-TAPT membranes. The preparation of COF Tp-TAPA and COF Tp-DAP is similar to the preparation of COF Tp-TAPT, only replacing TAPT with TAPA (10 mM) and DAP (15 mM).

OSN performance tests

The separation tests were carried out on a homemade dead-end setup. Before testing, the membrane was compacted for more than 30 min at 2 bar to reach a steady state. The permeance (J, kg m^{-2} $hour^{-1}$) was calculated by Eq. 1

$$J = \frac{M}{S \times t \times P} \quad (1)$$

where M (kg) is the weight of filtrate solution collected from the permeate side, S (m^2) denotes the effective area of the membrane used for separation, t (hours) presents the according test time, and P (bar) describes the transmembrane pressure. Rejection (R, %) of dyes was calculated by Eq. 2, where C_p and C_f are the solute concentrations in permeate and feed, respectively

$$R = \left(1 - \frac{C_P}{C_f}\right) \times 100 \quad (2)$$

The permeate samples were collected at least three times to obtain the average values and SDs of the final results.

MWCO analysis test procedure

The MWCO of COF membranes was estimated from the rejection of dye molecules with different molecular weights in specific solvents. Chrysoidine G (248.7 Da), methyl orange (327.3 Da), acid blue 25 (416.4 Da), acid fuchsin (585.5 Da), Congo red (696.7 Da), and methyl blue (799.8 Da) were used as markers of OSN experiment. The concentrations of feed, permeate, and retentate solutions were measured from the intensity of the characteristic UV-Vis absorption peaks after half or one-fourth dilution (when required). The MWCO is the minimum molecular weight of a solute that is 90% retained by the membrane, which was obtained by the plot of rejection of dye molecules against their molecular weights.

Molecular simulations of COF films

Molecular simulations of COF films were carried out in the software package of Materials Studio [2017 R2(17.2.0.1626) version, Accelrys Software Inc.]. The $P1$ space group was used for all the quasi-AB–stacking structures in the present study. To identify the model with predicted PXRD patterns that best match the experimental result, we used powder diffraction with the "mirror diffraction" function. With this function, the predicted PXRD pattern can change automatically with the variation of model structures. Therefore, by continuously adjusting the model structure, we can compare the PXRD patterns of almost every possible interlayer-shifted COF structure with the experimental data and finally identify the one particular structure that best matches the experimental result. Theoretical models were optimized by the Forcite module. The COMPASS II force field implemented in the Forcite module was used. The method of x-ray diffraction was used to simulate the powder diffraction of the COFs. Pawley refinements of the PXRD patterns were conducted in the Reflex module using 2θ data from 1.5° to 40°. The integrated intensities were extracted with the Pseudo-Voigt profile. As for the dried COFs, the unit cell parameters a, b, and c, full width at half maximum parameters U, V, and W, profile parameters NA and NB, and zero point were refined based on previous studies (*57*–*60*). As for the solvated COFs, in addition to the above parameters, α, β, and γ parameters were also refined. The background was refined with 20th-order polynomial.

First-principles DFT calculations were performed in Castep software [Materials Studio, 2017 R2(17.2.0.1626) version, Accelrys Software Inc.]. A semiempirical addition of dispersive forces to conventional DFT was included in the calculation to account for van der Waals interactions. Vanderbilt-type ultrasoft pseudopotentials and generalized gradient approximation (GGA) with a Perdew-Burke-Ernzerhof (PBE) exchange correlation and norm-conserving Troullier-Martins pseudopotentials in Kleinman-Bylander factorized form were used. In all calculations, we used periodic boundary conditions and a 3 × 3 × 4 supercell to present the full coordination environments of COFs. The plane-wave energy cutoff of 400 eV was used. The Brillouin zone of the 2D structures was sampled with 64 k-points (generated using the Monkhorst-Pack scheme), which ensures the convergence of the calculated total energies within 0.01 meV $atom^{-1}$. The atomic coordinates and unit-cell vectors were considered optimized when the remnant force on each atom was less than 0.04 eV/Å. The structures of the simulated AA-stacked and quasi-AB–stacked COFs were first optimized, and then solvent molecules were introduced to various locations of the channel pore, followed by a full structural relaxation to obtain a stable state of the material loaded with solvent molecules. To obtain the solvent binding energy, an isolated solvent molecule placed in a supercell (with the same cell dimensions as the material crystal) was also relaxed as a reference.

Supplementary Materials

This PDF file includes:

Supplementary Materials and Methods
Supplementary Text
Figs. S1 to S43
Tables S1 and S2
References

REFERENCES AND NOTES

1. M. Buonomenna, J. Bae, Organic solvent nanofiltration in pharmaceutical industry. *Sep. Purif. Rev.* **44**, 157–182 (2015).
2. P. Marchetti, M. F. J. Solomon, G. Szekely, A. G. Livingston, Molecular separation with organic solvent nanofiltration: A critical review. *Chem. Rev.* **114**, 10735–10806 (2014).
3. R. P. Lively, D. S. Sholl, From water to organics in membrane separations. *Nat. Mater.* **16**, 276–279 (2017).
4. K. Vanherck, G. Koeckelberghs, I. F. J. Vankelecom, Crosslinking polyimides for membrane applications: A review. *Prog. Polym. Sci.* **38**, 874–896 (2013).
5. Z. P. Liao, J. Y. Zhu, X. Li, B. Van der Bruggen, Regulating composition and structure of nanofillers in thin film nanocomposite (TFN) membranes for enhanced separation performance: A critical review. *Sep. Purif. Technol.* **266**, 21 (2021).
6. S. Karan, Z. Jiang, A. G. Livingston, Sub–10 nm polyamide nanofilms with ultrafast solvent transport for molecular separation. *Science* **348**, 1347–1351 (2015).
7. M. H. Abdellah, L. Perez-Manriquez, T. Puspasari, C. A. Scholes, S. E. Kentish, K. V. Peinemann, A catechin/cellulose composite membrane for organic solvent nanofiltration. *J. Membr. Sci.* **567**, 139–145 (2018).
8. J. Aburabie, K. V. Peinemann, Crosslinked poly(ether block amide) composite membranes for organic solvent nanofiltration applications. *J. Membr. Sci.* **523**, 264–272 (2017).
9. C. Li, S. X. Li, L. Lv, B. W. Su, M. Z. Hu, High solvent-resistant and integrally crosslinked polyimide-based composite membranes for organic solvent nanofiltration. *J. Membr. Sci.* **564**, 10–21 (2018).
10. B. Sengupta, Q. B. Dong, R. Khadka, D. K. Behera, R. Z. Yang, J. Liu, J. Jiang, P. Keblinski, G. Belfort, M. Yu, Carbon-doped metal oxide interfacial nanofilms for ultrafast and precise separation of molecules. *Science* **381**, 1098–1104 (2023).

11. G. M. Shi, Y. N. Feng, B. F. Li, H. M. Tham, J. Y. Lai, T. S. Chun, Recent progress of organic solvent nanofiltration membranes. *Prog. Polym. Sci.* **123**, 27 (2021).
12. H. J. Wang, M. D. Wang, X. Liang, J. Q. Yuan, H. Yang, S. Y. Wang, Y. X. Ren, H. Wu, F. S. Pan, Z. Y. Jiang, Organic molecular sieve membranes for chemical separations. *Chem. Soc. Rev.* **50**, 5468–5516 (2021).
13. A. He, Z. W. Jiang, Y. Wu, H. Hussain, J. Rawle, M. E. Briggs, M. A. Little, A. G. Livingston, A. I. Cooper, A smart and responsive crystalline porous organic cage membrane with switchable pore apertures for graded molecular sieving. *Nat. Mater.* **21**, 463–470 (2022).
14. Z. F. Wang, Q. Yu, Y. B. Huang, H. D. An, Y. Zhao, Y. F. Feng, X. Li, X. L. Shi, J. J. Liang, F. S. Pan, P. Cheng, Y. Chen, S. Q. Ma, Z. J. Zhang, PolyCOFs: A new class of freestanding responsive covalent organic framework membranes with high mechanical performance. *ACS Central Sci.* **5**, 1352–1359 (2019).
15. C. S. Diercks, O. M. Yaghi, The atom, the molecule, and the covalent organic framework. *Science* **355**, eaal1585 (2017).
16. U. Diaz, A. Corma, Ordered covalent organic frameworks, COFs and PAFs. From preparation to application. *Coord. Chem. Rev.* **311**, 85–124 (2016).
17. A. P. Cote, A. I. Benin, N. W. Ockwig, M. O'Keeffe, A. J. Matzger, O. M. Yaghi, Porous, crystalline, covalent organic frameworks. *Science* **310**, 1166–1170 (2005).
18. N. Huang, P. Wang, D. L. Jiang, Covalent organic frameworks: A materials platform for structural and functional designs. *Nat. Rev. Mater.* **1**, 16068 (2016).
19. S. Yuan, X. Li, J. Zhu, G. Zhang, P. Van Puyvelde, B. Van der Bruggen, Covalent organic frameworks for membrane separation. *Chem. Soc. Rev.* **48**, 2665–2681 (2019).
20. M. Matsumoto, L. Valentino, G. M. Stiehl, H. B. Balch, A. R. Corcos, F. Wang, D. C. Ralph, B. J. Marinas, W. R. Dichtel, Lewis-acid-catalyzed interfacial polymerization of covalent organic framework films. *Chem* **4**, 308–317 (2018).
21. M. Wang, P. Zhang, X. Liang, J. Zhao, Y. Liu, Y. Cao, H. Wang, Y. Chen, Z. Zhang, F. Pan, Ultrafast seawater desalination with covalent organic framework membranes. *Nat. Sustain.* **5**, 518–526 (2022).
22. C. J. Kang, Z. Q. Zhang, V. Wee, A. K. Usadi, D. C. Calabro, L. S. Baugh, S. Wang, Y. X. Wang, D. Zhao, Interlayer shifting in two-dimensional covalent organic frameworks. *J. Am. Chem. Soc.* **142**, 12995–13002 (2020).
23. L. Wang, J. L. He, M. Heiranian, H. Q. Fan, L. F. Song, Y. Li, M. Elimelech, Water transport in reverse osmosis membranes is governed by pore flow, not a solution-diffusion mechanism. *Sci. Adv.* **9**, eadf8488 (2023).
24. J. L. He, H. Q. Fan, M. Elimelech, Y. Li, Molecular simulations of organic solvent transport in dense polymer membranes: Solution-diffusion or pore-flow mechanism? *J. Membr. Sci.* **708**, 12 (2024).
25. H. Q. Fan, J. L. He, M. Heiranian, W. Y. Pan, Y. Li, M. Elimelech, The physical basis for solvent flow in organic solvent nanofiltration. *Sci. Adv.* **10**, eado4332 (2024).
26. L. Peeva, J. Da Silva Burgal, Z. Heckenast, F. Brazy, F. Cazenave, A. Livingston, Continuous consecutive reactions with inter-reaction solvent exchange by membrane separation. *Angew. Chem. Int. Edit.* **55**, 13576–13579 (2016).
27. A. V. Volkov, V. V. Parashchuk, D. F. Stamatialis, V. S. Khotimsky, V. V. Volkov, M. Wessling, High permeable PTMSP/PAN composite membranes for solvent nanofiltration. *J. Membr. Sci.* **333**, 88–93 (2009).
28. S. Tsarkov, V. Khotimskiy, P. M. Budd, V. Volkov, J. Kukushkina, A. Volkov, Solvent nanofiltration through high permeability glassy polymers: Effect of polymer and solute nature. *J. Membr. Sci.* **423**, 65–72 (2012).
29. D. Fritsch, P. Merten, K. Heinrich, M. Lazar, M. Priske, High performance organic solvent nanofiltration membranes: Development and thorough testing of thin film composite membranes made of polymers of intrinsic microporosity (PIMs). *J. Membr. Sci.* **401**, 222–231 (2012).
30. Z. Ali, B. S. Ghanem, Y. Wang, F. Pacheco, W. Ogieglo, H. Vovusha, G. Genduso, U. Schwingenschlögl, Y. Han, I. Pinnau, Finely tuned submicroporous thin-film molecular sieve membranes for highly efficient fluid separations. *Adv. Mater.* **32**, e2001132 (2020).
31. J. Li, M. Zhang, W. Feng, L. Zhu, L. Zhang, PIM-1 pore-filled thin film composite membranes for tunable organic solvent nanofiltration. *J. Membr. Sci.* **601**, 117951 (2020).
32. J. Geens, K. Peeters, B. Van der Bruggen, C. Vandecasteele, Polymeric nanofiltration of binary water–alcohol mixtures: Influence of feed composition and membrane properties on permeability and rejection. *J. Membr. Sci.* **255**, 255–264 (2005).
33. Y. Wang, S. H. Goh, T. S. Chung, P. Na, Polyamide-imide/polyetherimide dual-layer hollow fiber membranes for pervaporation dehydration of C1–C4 alcohols. *J. Membr. Sci.* **326**, 222–233 (2009).
34. Z. F. Gao, G. M. Shi, Y. Cui, T.-S. Chung, Organic solvent nanofiltration (OSN) membranes made from plasma grafting of polyethylene glycol on cross-linked polyimide ultrafiltration substrates. *J. Membr. Sci.* **565**, 169–178 (2018).
35. K. Vanherck, S. Hermans, T. Verbiest, I. Vankelecom, Using the photothermal effect to improve membrane separations via localized heating. *J. Mater. Chem.* **21**, 6079–6087 (2011).
36. D. Y. Xing, S. Y. Chan, T.-S. Chung, The ionic liquid [EMIM] OAc as a solvent to fabricate stable polybenzimidazole membranes for organic solvent nanofiltration. *Green Chem.* **16**, 1383–1392 (2014).
37. B. Zhao, G. M. Shi, K. Y. Wang, J.-Y. Lai, T.-S. Chung, Employing a green cross-linking method to fabricate polybenzimidazole (PBI) hollow fiber membranes for organic solvent nanofiltration (OSN). *Sep. Purif. Technol.* **255**, 117702 (2021).
38. M. Mertens, C. Van Goethem, M. Thijs, G. Koeckelberghs, I. F. Vankelecom, Crosslinked PVDF-membranes for solvent resistant nanofiltration. *J. Membr. Sci.* **566**, 223–230 (2018).
39. H. M. Tham, K. Y. Wang, D. Hua, S. Japip, T.-S. Chung, From ultrafiltration to nanofiltration: Hydrazine cross-linked polyacrylonitrile hollow fiber membranes for organic solvent nanofiltration. *J. Membr. Sci.* **542**, 289–299 (2017).
40. K. Vanherck, T. Verbiest, I. Vankelecom, Comparison of two synthesis routes to obtain gold nanoparticles in polyimide. *J. Phys. Chem. C* **116**, 115–125 (2012).
41. L. Zhu, H. Yu, H. Zhang, J. Shen, L. Xue, C. Gao, B. van der Bruggen, Mixed matrix membranes containing MIL-53 (Al) for potential application in organic solvent nanofiltration. *RSC Adv.* **5**, 73068–73076 (2015).
42. Z. Wang, Z. Si, D. Cai, G. Li, S. Li, P. Qin, T. Tan, Improving ZIF-8 stability in the preparation process of polyimide-based organic solvent nanofiltration membrane. *Sep. Purif. Technol.* **227**, 115687 (2019).
43. Y. Li, H. Mao, H. Zhang, G. Yang, R. Ding, J. Wang, Tuning the microstructure and permeation property of thin film nanocomposite membrane by functionalized inorganic nanospheres for solvent resistant nanofiltration. *Sep. Purif. Technol.* **165**, 60–70 (2016).
44. K. Vanherck, I. Vankelecom, T. Verbiest, Improving fluxes of polyimide membranes containing gold nanoparticles by photothermal heating. *J. Membr. Sci.* **373**, 5–13 (2011).
45. Y. C. Xu, Y. P. Tang, L. F. Liu, Z. H. Guo, L. Shao, Nanocomposite organic solvent nanofiltration membranes by a highly-efficient mussel-inspired co-deposition strategy. *J. Membr. Sci.* **526**, 32–42 (2017).
46. M. H. D. A. Farahani, D. Hua, T.-S. Chung, Cross-linked mixed matrix membranes consisting of carboxyl-functionalized multi-walled carbon nanotubes and P84 polyimide for organic solvent nanofiltration (OSN). *Sep. Purif. Technol.* **186**, 243–254 (2017).
47. M. H. D. A. Farahani, D. Hua, T.-S. Chung, Cross-linked mixed matrix membranes (MMMs) consisting of amine-functionalized multi-walled carbon nanotubes and P84 polyimide for organic solvent nanofiltration (OSN) with enhanced flux. *J. Membr. Sci.* **548**, 319–331 (2018).
48. H. Abadikhah, E. N. Kalali, S. Behzadi, S. A. Khan, X. Xu, M. E. Shabestari, S. Agathopoulos, High flux thin film nanocomposite membrane incorporated with functionalized TiO2@ reduced graphene oxide nanohybrids for organic solvent nanofiltration. *Chem. Eng. Sci.* **204**, 99–109 (2019).
49. T. Gao, L. Huang, C. Li, G. Xu, G. Shi, Graphene membranes with tuneable nanochannels by intercalating self-assembled porphyrin molecules for organic solvent nanofiltration. *Carbon* **124**, 263–270 (2017).
50. B. Li, Y. Cui, S. Japip, Z. Thong, T.-S. Chung, Graphene oxide (GO) laminar membranes for concentrating pharmaceuticals and food additives in organic solvents. *Carbon* **130**, 503–514 (2018).
51. D. Hua, T.-S. Chung, Polyelectrolyte functionalized lamellar graphene oxide membranes on polypropylene support for organic solvent nanofiltration. *Carbon* **122**, 604–613 (2017).
52. Y. Gao, K. Su, Z. Li, B. Cheng, Graphene oxide hybrid poly (p-phenylene sulfide) nanofiltration membrane intercalated by bis (triethoxysilyl) ethane. *Chem. Eng. J.* **352**, 10–19 (2018).
53. Y. Li, L. H. Wee, A. Volodin, J. A. Martens, I. F. Vankelecom, Polymer supported ZIF-8 membranes prepared via an interfacial synthesis method. *Chem. Commun.* **51**, 918–920 (2015).
54. D. Ma, G. Han, Z. F. Gao, S. B. Chen, Continuous UiO-66-type metal–organic framework thin film on polymeric support for organic solvent nanofiltration. *ACS Appl. Mater. Interfaces* **11**, 45290–45300 (2019).
55. X. Yu, W. Fan, V. Wee, D. Shi, H. Yuan, Y. Ying, Y. Di Yuan, Z. Yang, Y. Feng, D. Sun, Polycrystalline iron (III) metal-organic framework membranes for organic solvent nanofiltration with high permeance. *J. Membr. Sci.* **644**, 120130 (2022).
56. K. Xu, B. Feng, C. Zhou, A. Huang, Synthesis of highly stable graphene oxide membranes on polydopamine functionalized supports for seawater desalination. *Chem. Eng. Sci.* **146**, 159–165 (2016).
57. B. J. Smith, A. C. Overholts, N. Hwang, W. R. Dichtel, Insight into the crystallization of amorphous imine-linked polymer networks to 2D covalent organic frameworks. *Chem. Commun.* **52**, 3690–3693 (2016).
58. J. Dong, Y. Wang, G. Liu, Y. Cheng, D. Zhao, Isoreticular covalent organic frameworks for hydrocarbon uptake and separation: The important role of monomer planarity. *CrstEngComm* **19**, 4899–4904 (2017).
59. H. Xu, J. Gao, D. Jiang, Stable, crystalline, porous, covalent organic frameworks as a platform for chiral organocatalysts. *Nat. Chem.* **7**, 905–912 (2015).
60. F. Auras, L. Ascherl, A. H. Hakimioun, J. T. Margraf, F. C. Hanusch, S. Reuter, D. Bessinger, M. Döblinger, C. Hettstedt, K. Karaghiosoff, Synchronized offset stacking: A concept for growing large-domain and highly crystalline 2D covalent organic frameworks. *J. Am. Chem. Soc.* **138**, 16703–16710 (2016).

61. L. Nie, C. Y. Chuah, T. H. Bae, J. M. Lee, Graphene-based advanced membrane applications in organic solvent nanofiltration. *Adv. Funct. Mater.* **31**, 2006949 (2021).
62. C. E. Webster, R. S. Drago, M. C. Zerner, Molecular dimensions for adsorptives. *J. Am. Chem. Soc.* **120**, 5509–5516 (1998).
63. A. F. Barton, Solubility parameters. *Chem. Rev.* **75**, 731–753 (1975).

Acknowledgments
Funding: This work was supported by the Centre for Hydrogen Innovations (CHI-P2024-01); the Ministry of Education—Singapore (MOE-T2EP10122-0002); the Energy Market Authority of Singapore (EMA-EP009-SEGC-020); the Agency for Science, Technology and Research (U2102d2004 and U2102d2012); and the National Research Foundation Singapore (NRF-CRP26-2021RS-0002 and NRF-NRFI08-2022-0008). **Author contributions:** D.Z. formulated and supervised the project. H.Y. designed the experiments. H.Y., C.K., and C.J. conducted the simulations. H.Y., H.Z., and D.S. conducted the membrane separation performance tests. All authors contributed to writing and revising the manuscript. **Competing interests:** H.Y. and D.Z. are inventors of a patent application (no. 10202402940W) filed by the National University of Singapore on 23 September 2024. The other authors declare that they have no competing interests. **Data and materials availability:** All data needed to evaluate the conclusions in the paper are present in the paper and/or the Supplementary Materials.

Submitted 25 July 2024
Accepted 13 November 2024
Published 18 December 2024
10.1126/sciadv.ads0260